Global Climate Impacts of Fixing the Southern Ocean Shortwave Radiation Bias in the Community Earth System Model (CESM)

JENNIFER E. KAY,[a] CASEY WALL,[b] VINEEL YETTELLA,[a] BRIAN MEDEIROS,[c] CECILE HANNAY,[c] PETER CALDWELL,[d] AND CECILIA BITZ[b]

[a] *Cooperative Institute for Research in Environmental Sciences, and Department of Atmospheric and Oceanic Sciences, University of Colorado Boulder, Boulder, Colorado*
[b] *Department of Atmospheric Sciences, University of Washington, Seattle, Washington*
[c] *Climate and Global Dynamics, National Center for Atmospheric Research,[e] Boulder, Colorado*
[d] *Livermore National Lab, Department of Energy, Livermore, California*

(Manuscript received 19 May 2015, in final form 21 March 2016)

ABSTRACT

A large, long-standing, and pervasive climate model bias is excessive absorbed shortwave radiation (ASR) over the midlatitude oceans, especially the Southern Ocean. This study investigates both the underlying mechanisms for and climate impacts of this bias within the Community Earth System Model, version 1, with the Community Atmosphere Model, version 5 [CESM1(CAM5)]. Excessive Southern Ocean ASR in CESM1(CAM5) results in part because low-level clouds contain insufficient amounts of supercooled liquid. In a present-day atmosphere-only run, an observationally motivated modification to the shallow convection detrainment increases supercooled cloud liquid, brightens low-level clouds, and substantially reduces the Southern Ocean ASR bias. Tuning to maintain global energy balance enables reduction of a compensating tropical ASR bias. In the resulting preindustrial fully coupled run with a brighter Southern Ocean and dimmer tropics, the Southern Ocean cools and the tropics warm. As a result of the enhanced meridional temperature gradient, poleward heat transport increases in both hemispheres (especially the Southern Hemisphere), and the Southern Hemisphere atmospheric jet strengthens. Because northward cross-equatorial heat transport reductions occur primarily in the ocean (80%), not the atmosphere (20%), a proposed atmospheric teleconnection linking Southern Ocean ASR bias reduction and cooling with northward shifts in tropical precipitation has little impact. In summary, observationally motivated supercooled liquid water increases in shallow convective clouds enable large reductions in long-standing climate model shortwave radiation biases. Of relevance to both model bias reduction and climate dynamics, quantifying the influence of Southern Ocean cooling on tropical precipitation requires a model with dynamic ocean heat transport.

1. Motivation

Excessive absorbed shortwave radiation (ASR) over the midlatitude oceans is a ubiquitous, large, and long-standing bias in both climate models and reanalyses (Trenberth and Fasullo 2010; Hwang and Frierson 2013). ASR biases are largest over the Southern Ocean, where local differences between satellite-observed and modeled ASR often reach tens ofwatts per square meter. In many models, insufficient cloud optical depth explains the excessive midlatitude ocean ASR. Simply put, the model clouds are not bright enough. Studies using cyclone compositing have shown that climate model ASR biases are largest in the post-cold-front regions of midlatitude cyclones where low-topped shallow convective clouds are the dominant cloud type (Bodas-Salcedo et al. 2014; Williams et al. 2013; Bodas-Salcedo et al. 2012).

Recognizing that large model radiation errors may have a profound influence on the simulated climate, this study has two goals. First, we aim to use observations to motivate improvements in climate model physics and reduce midlatitude ocean ASR bias. Second, we aim to

Supplemental information related to this paper is available at the Journals Online website: http://dx.doi.org/10.1175/JCLI-D-15-0358.s1.

[e] The National Center for Atmospheric Research is sponsored by the National Science Foundation.

Corresponding author address: Jennifer E. Kay, CIRES/ATOC, University of Colorado Boulder, 216 UCB, Boulder, CO 80309.
E-mail: jennifer.e.kay@colorado.edu

DOI: 10.1175/JCLI-D-15-0358.1

assess the impacts of reduced midlatitude ocean ASR bias on global climate. To achieve these goals, we employ a widely used global coupled climate model: the Community Earth System Model, version 1, with the Community Atmosphere Model, version 5 [CESM1(CAM5); Hurrell et al. 2013]. Like most climate models of its class, CESM1(CAM5) has excessive midlatitude ocean ASR as a result of dim clouds that do not scatter enough incoming sunlight back to space (Kay et al. 2012a).

Accomplishing the first goal of this study requires identifying and removing a deficiency in the model equations used to predict midlatitude ocean cloud properties. Satellite and in situ observations show ubiquitous supercooled cloud liquid in low-level clouds over the midlatitude oceans, especially the Southern Ocean (e.g., Hu et al. 2010; Morrison et al. 2011; Huang et al. 2012; Cesana and Chepfer 2013; Chubb et al. 2013; Bodas-Salcedo et al. 2016). Even close to the Antarctic continent during winter, total glaciation in low clouds over the Southern Ocean is rare (e.g., Morrison et al. 2011; Huang et al. 2012). Supercooled cloud liquid exerts a strong control on cloud radiative effects in both models (e.g., Kay et al. 2014; Forbes and Ahlgrimm 2014) and observations (e.g., Shupe and Intrieri 2004; Bodas-Salcedo et al. 2016).

Numerical weather and climate models struggle to reproduce observations of ubiquitous supercooled liquid-containing clouds in the extratropical atmosphere (e.g., Cesana and Chepfer 2013; Forbes and Ahlgrimm 2014; Gettelman et al. 2015). The processes that produce and remove supercooled cloud liquid are not explicitly resolved in these models because they occur at a scale that is much smaller than the model resolution. But beyond this scale challenge, it is important to realize that the ubiquitous presence of supercooled liquid is in itself surprising and not fully understood (Morrison et al. 2012). It is well known that when ice and supercooled liquid coexist, the ice grows at the expense of the liquid by the Wegener–Bergeron–Findeisen mechanism (Wegener 1911; Bergeron 1935; Findeisen 1938). Indeed, the turbulent and microphysical processes that enable supercooled liquid to persist in the atmosphere despite the Wegener–Bergeron–Findeisen mechanism are complex, coupled, and enigmatic.

Motivated by observations of ubiquitous supercooled liquid in midlatitude oceanic clouds and by knowing that cloud liquid water content exerts a strong control on cloud radiative properties, we propose a hypothesis: midlatitude ocean clouds are not bright enough in climate models because the modeled clouds contain insufficient amounts of supercooled liquid water. To test this hypothesis, we change the model physics in CESM1(CAM5) to allow more supercooled liquid water in shallow convective clouds (see supplemental information). In support of our hypothesis, increasing supercooled liquid in shallow convective clouds makes those clouds brighter and substantially reduces the excessive midlatitude oceanic ASR bias, especially over the Southern Ocean.

Having introduced our first goal, we next introduce and motivate our second goal: documenting the influence of midlatitude ocean ASR bias reduction on the global climate system. Given the large magnitude of the ASR biases we aim to reduce, we expect bias reduction will produce changes in global energy budgets and in atmospheric and oceanic circulation. In particular, we investigate the possibility that brightening midlatitude clouds will lead to a tropical precipitation response via an atmospheric teleconnection. As described in recent review papers by Chiang and Friedman (2012) and Schneider et al. (2014), the central idea behind this atmospheric teleconnection is simple: a hemispheric asymmetry in heating or cooling shifts tropical rainfall and associated atmospheric circulation toward the relatively warmed hemisphere. Especially pertinent to this study, Hwang and Frierson (2013) invoke this atmospheric teleconnection when hypothesizing that fixing the Southern Ocean ASR climate model bias will preferentially cool the Southern Hemisphere and shift tropical precipitation northward to ameliorate another long-standing climate model bias: the double intertropical convergence zone (ITCZ) bias (e.g., Lin 2007). We test this proposed extratropical–tropical teleconnection in a hierarchy of model configurations with varying degrees of atmosphere–ocean coupling. As we will show, dynamic ocean heat transport mutes the atmospheric teleconnection linking Southern Ocean cooling with northward ITCZ shifts.

2. Model and experiments

a. *Midlatitude oceanic clouds in CESM1(CAM5)*

We use a single climate model for our numerical experiments: CESM1(CAM5). All of our numerical experiments were done with the CESM Large Ensemble project (CESM-LE) code base (Kay et al. 2015), which uses CAM, version 5.2. CESM1(CAM5) is a state-of-the-art global coupled climate model that participated in phase 5 of the Coupled Model Intercomparison Project (CMIP5; Taylor et al. 2012). A full description of CESM1(CAM5) and its capabilities can be found in a special collection of the *Journal of Climate*. Of particular relevance to this study are the representation of double-moment cloud microphysics (Morrison and Gettelman 2008) and shallow convection (Park and Bretherton 2009). A description of the integration of cloud processes in CAM5 can be found in Park et al. (2014).

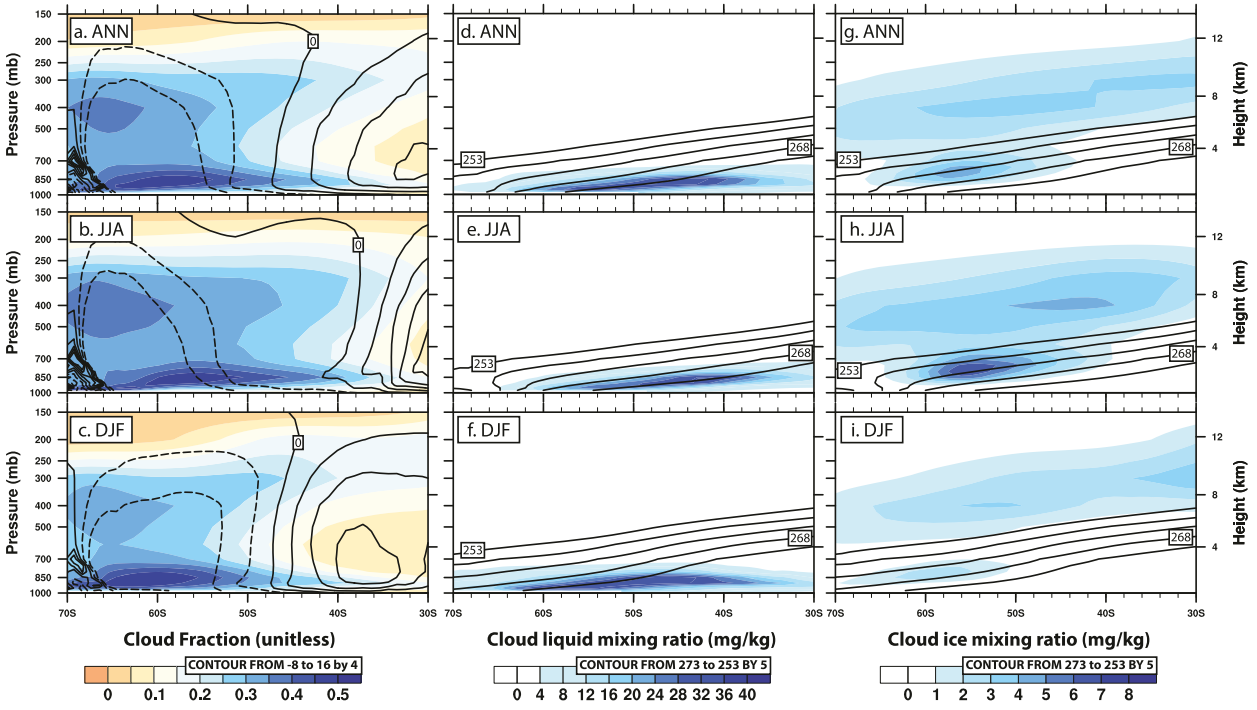

FIG. 1. Atmospheric circulation, clouds, and air temperatures over the Southern Ocean in the fully coupled control run (FC1850_cnt; Table 1). (left) Cloud fraction (colors) and subsidence (black contours; hPa day^{-1}) for the (a) annual mean (ANN), (b) Southern Hemisphere winter (JJA), and (c) Southern Hemisphere summer (DJF). (center) Gridbox cloud liquid mixing ratio (colors) and air temperature (black contours; K) for (d) ANN, (e) JJA, and (f) DJF. (g)–(i) As in (d)–(f), but for cloud ice mixing ratio.

To introduce midlatitude oceanic regions in CESM1(CAM5), Figs. 1a–c show the atmospheric circulation and cloud distribution from 30° to 70°S for the annual mean, Southern Hemisphere winter (JJA), and Southern Hemisphere summer (DJF). In the annual mean, ascent from 50° to 70°S associated with the midlatitude storm track leads to relatively large cloud fractions from the surface into the free troposphere, with the largest cloud fractions below 700 mb (1 mb = 1 hPa). From 30° to 50°S, subsidence associated with the descending branch of the Hadley circulation leads to relatively small cloud fractions throughout the troposphere and relatively shallow low cloud tops. Seasonal changes in insolation shift the entire atmospheric circulation pattern poleward in DJF and equatorward in JJA, but the general nature of the circulation and corresponding cloud distributions are seasonally invariant.

In addition to cloud fraction, cloud properties (e.g., phase, temperature, and particle size) exert a strong control on cloud radiative effects. For example, Southern Ocean total cloud fractions within CAM5 are within 0.10 of satellite observations, yet CAM5 still has large Southern Ocean ASR biases indicative of cloud properties biases (Kay et al. 2012a). Motivated by the need to understand cloud properties and specifically cloud water content, Figs. 1d–i show the vertical distribution of Southern Ocean cloud water content in CESM1(CAM5) in the annual mean, DJF, and JJA. At all times of the year, the vast majority of the CESM1(CAM5) low-level (pressure > 700 mb) cloud water is liquid, not ice. Supercooled liquid dominates between 268 and 273 K. Below 268 K, the cloud water content is a mix of water and ice. Observations show supercooled liquid dominance down to 253 K (Hu et al. 2010; Morrison et al. 2011; Cesana and Chepfer 2013; Chubb et al. 2013). Indeed, comparisons with satellite observations (Cesana and Chepfer 2013; O'Dell et al. 2008) show that CAM5 clouds have too much ice and insufficient supercooled cloud liquid over the Southern Ocean (Kay et al. 2016). In summary, CESM1(CAM5) contains insufficient supercooled cloud liquid at temperatures below 268 K.

Having identified that CESM1(CAM5) clouds have insufficient supercooled cloud liquid, how can this cloud phase bias be "fixed"? Cloud properties in climate models are controlled by interactions between the grid-scale processes, such as condensation and evaporation, and the parameterized physics, most notably the cloud microphysics and convection. The dominant processes controlling modeled clouds can be identified using

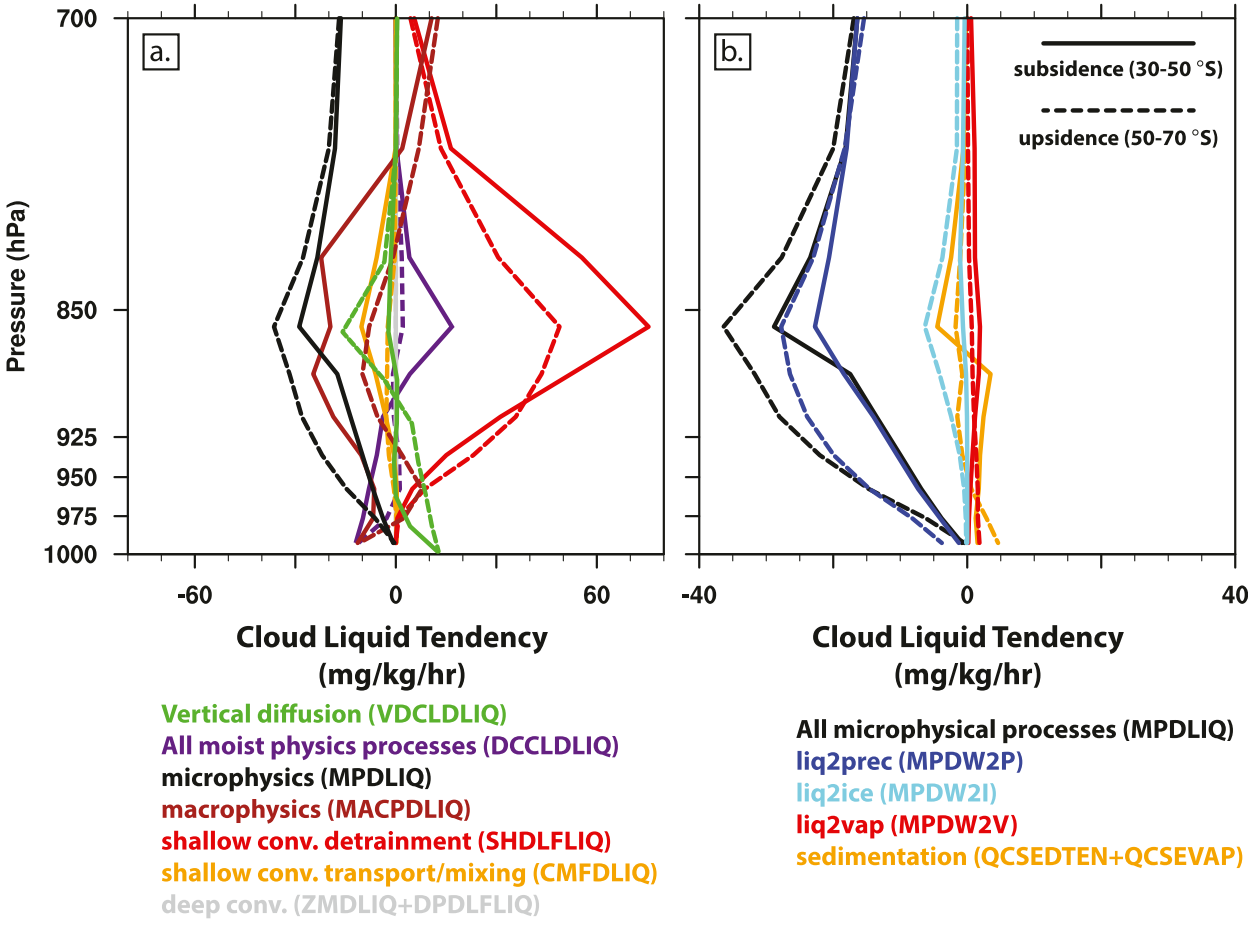

FIG. 2. Annual mean cloud liquid tendencies over the subsidence (30°–50°S, solid) and ascent (50°–70°S, dashed) regions of the Southern Ocean in the fully coupled control run (FC1850_cnt; Table 1): (a) vertical diffusion and all moist physics tendencies; (b) microphysics tendencies. Note: the total tendency due to moist physics processes is the sum of MPDLIQ, MACPDLIQ, SHDLFLIQ CMFDLIQ, ZMDLIQ, and DPDLFLIQ. The total tendency due to microphysical processes is the sum of MPDW2P, MPDW2I, MPDW2V, QCSEDTEN, and QCSEVAP.

tendencies: namely, the change in cloud mixing ratio per unit time resulting from the physical processes represented by the model.

Figure 2 shows the annual mean cloud liquid tendencies in both the subsidence (30°–50°S) and ascent (50°–70°S) regions for CESM1(CAM5) moist physical processes. Over both Southern Ocean regions, detrainment from the shallow convection parameterization (SHDLFLIQ) is the primary source of low-level cloud condensate. Once liquid cloud forms, it is depleted by precipitation in the parameterized microphysics (MPDW2P); grid-scale evaporation, also known as ''the macrophysics'' (MACPDLIQ); and, to a lesser extent, by convective transport–mixing (entrainment of dry air) in the parameterized shallow convection (CMFDLIQ). The conversion of cloud liquid to precipitation (MPDW2P) primarily produces rain but also some snow in the ascent regime (not shown). Conversion of cloud liquid to ice (MPDW2I), which occurs primarily via the Wegener–Bergeron–Findeisen process (not shown), is a secondary sink for cloud liquid in the ascent regime (Fig. 2b). In the ascent regime, vertical diffusion (turbulent mixing) is also a sink for cloud liquid produced by moist physical processes (not shown). Deep convection has a negligible influence on Southern Ocean cloud liquid, and thus deep convective tendencies are small.

Since cloud liquid and ice water content are governed by complex prognostic equations involving many processes, coming up with a simple explanation for insufficient supercooled liquid in CAM5 at first seems hopeless. Knowing that shallow convective detrainment is the primary source of Southern Ocean cloud liquid (Fig. 2) is extremely helpful in this regard. Indeed, knowing that shallow convective detrainment is the primary source of Southern Ocean cloud liquid (Fig. 2) helps explain why most of the supercooled cloud liquid

TABLE 1. Description of global climate model runs. All runs use the Community Earth System Model with the Community Atmosphere Model, version 5 [CESM1(CAM5); Hurrell et al. 2013] at 1° horizontal resolution with the finite-volume dynamical core.

Name	Length (yr)	Climate forcing (year)	Description
ATM2000_cnt	10	2000	Atmosphere-only control with prescribed 2000 surface ocean.
ATM2000_exp	10	2000	Atmosphere-only experiment (T_{ice} = 253 K) with prescribed 2000 surface ocean.
FC1850_cnt	29	1850	Fully coupled control; initial condition 1 Jan, year 402 of CESM-LE 1850 control run b.e11.B1850C5CN.f09_g16.005 (Kay et al. 2015).
FC1850_exp	29	1850	Fully coupled experiment (T_{ice} = 253 K); initial condition 1 Jan, year 402 of CESM-LE 1850 control run b.e11.B1850C5CN.f09_g16.005.
FC1850_texp	200	1850	Fully coupled tuned experiment (T_{ice} = 253 K); initial condition 1 Jan, year 402 of CESM-LE 1850 control run b.e11.B1850C5CN.f09_g16.005.
SOM1850_cnt	20	1850	Slab ocean model control with prescribed ocean heat transport from FC1850_cnt; initial condition 1 Jan, year 402 of CESM-LE 1850 control run b.e11.B1850C5CN.f09_g16.005.
SOM1850_texp_ocnht=texp	20	1850	Slab ocean model tuned experiment (T_{ice} = 253 K) with prescribed ocean heat transport from FC1850_texp; initial condition 1 Jan, year 150 of FC1850_texp.
SOM1850_texp_ocnht=cnt	20	1850	Slab ocean model tuned experiment (T_{ice} = 253 K) with prescribed ocean heat transport from FC1850_cnt; initial condition 1 Jan, year 402 of CESM-LE 1850 control run b.e11.B1850C5CN.f09_g16.005.

occurs between temperatures of 268 and 273 K (Fig. 1). While the cloud microphysics predicts cloud phase, the shallow convection prescribes cloud phase for the detrained condensate that forms cloud using a piecewise linear function of temperature:

$$f = 0; \quad \text{for} \quad T > T_{ice},$$
$$f = (T_{ice} - T)/30; \quad \text{for} \quad 238.15\,\text{K} < T < T_{ice}, \quad \text{and}$$
$$f = 1; \quad \text{for} \quad T < 238.15\,\text{K} \tag{1}$$

where f is the glaciated fraction (unitless), T is temperature (kelvin), and T_{ice} is a constant that specifies the temperature below which the shallow convection detrains ice (kelvin). In the default configuration, T_{ice} = 268 K. In other words, detrained condensate below 268 K contains ice, but above 268 K all detrained condensate is liquid.

Because the shallow convection is the primary source of low-level cloud condensate over the midlatitude oceans, changing T_{ice} in Eq. (1) provides a simple lever to change the amount of supercooled liquid in shallow convective clouds. Motivated by observations showing supercooled liquid dominates at temperatures well below 268 K, we conduct experiments in which we increase the supercooled liquid detrained from shallow convection by changing T_{ice}. Consistent with Figs. 1 and 2, changing T_{ice} from 268 to 253 K implies that a much larger fraction of the cloud condensate detrained by the shallow convection will be liquid over the Southern Ocean. We note that changing T_{ice} has no effect on low-level tropical clouds with cloud-top temperatures that exceed 273 K. We also note that T_{ice} = 253 K was the original value proposed by Park and Bretherton (2009), but it was not adopted as the default value during CESM1(CAM5) development.

b. CESM1(CAM5) runs used for this study

We next introduce the model runs used in this study (Table 1). To accomplish goal 1—testing the hypothesis that increasing supercooled liquid in detrained condensate from the shallow convection reduces the excessive midlatitude ocean ASR bias in CESM1(CAM5)—we use atmosphere-only runs with fixed year 2000 sea ice and ocean conditions. Atmosphere-only runs have prognostic atmosphere and land but prescribed surface ocean conditions and no ocean heat transport. Atmosphere-only runs are useful for quantifying model biases resulting from the model representation of atmospheric processes. For example, CESM1(CAM5) has excessive Antarctic sea ice, a bias that complicates interpretation of ASR bias at high Southern Ocean latitudes. We completed both a "control" atmosphere-only CAM5 run in which the physics is identical to the released version of CESM1(CAM5) and an "experiment" atmosphere-only CAM5 run in which we decreased T_{ice} from its control value of 268 K to its experiment value of 253 K [see Eq. (1)]. To test our hypothesis, we evaluate top-of-atmosphere ASR biases by comparing model runs to satellite-observed radiative fluxes from version 2.8 of the Clouds and the Earth's Radiant Energy System–Energy Balanced and Filled (CERES-EBAF) dataset (Loeb et al. 2009).

To accomplish goal 2—evaluating the impact of reduced midlatitude ocean ASR bias on global climate—we use fully coupled CESM1(CAM5) simulations with constant 1850 climate conditions starting with initial conditions

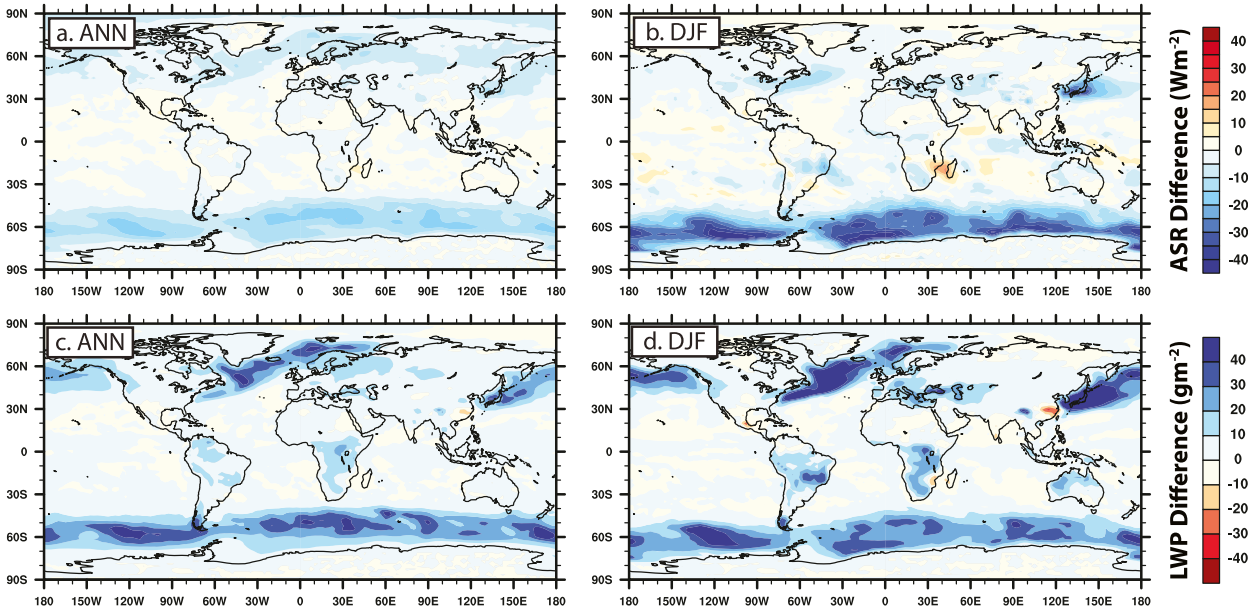

FIG. 3. Global difference maps for atmosphere-only runs (ATM2000_exp minus ATM2000_cnt): (a) ASR difference for ANN. (b) As in (a), but for DJF. (c) ANN gridbox mean cloud LWP. (d) As in (c), but for DJF. See Table 1 for model run descriptions.

from 1 January, year 402 from the 1850 fully coupled control run of the CESM-LE project (Kay et al. 2015). Fully coupled models have prognostic atmosphere, ocean, land, and sea ice component models and, as such, can predict changes in atmosphere and ocean heat transport in response to model physics changes like those proposed here. Like the atmosphere-only runs, we completed fully coupled runs with differing values of T_{ice}. To complement the fully coupled runs, we completed slab ocean model (SOM) runs. SOM runs have prognostic mixed layer ocean and sea ice but constant prescribed ocean heat transport. As a result, SOM runs come into equilibrium on the time scales of the mixed-layer ocean (decades, proportional to the mixed-layer heat capacity) as opposed to the time scales of the deep ocean (centuries or greater). We use the SOM runs to identify the importance of ocean heat transport for the model climate response to ASR bias reduction.

3. Results

a. *Shortwave radiation bias reduction in atmosphere-only runs*

We begin by presenting ASR bias in present-day atmosphere-only runs. We compare the control with T_{ice} = 268 K (ATM2000_cnt) to the experiment with T_{ice} = 253 K (ATM2000_exp; Table 1). Decreasing T_{ice} increases the cloud liquid water path (LWP) and decreases ASR over the midlatitude oceans in both hemispheres where shallow convective clouds dominate (Fig. 3a). At Southern Hemisphere midlatitudes, oceans are the dominant surface type, and there is an active storm track year round. As a result, we find decreasing T_{ice} leads to the largest ASR bias reductions over the Southern Ocean. Not surprisingly, global maps show the largest Southern Ocean ASR reductions occur in Southern Hemisphere summer (DJF) (Fig. 3b). In the North Atlantic and North Pacific, ASR reductions occur in transition seasons (MAM and SON), but not during Northern Hemisphere summer (JJA), when many shallow convective midlatitude clouds have temperatures above 273 K and midlatitude cyclone activity is reduced (not shown).

Focusing on the region with the largest ASR bias and bias reduction, we next compare zonal mean ASR model bias in the control and the experiment over the Southern Ocean (Fig. 4). Increasing the supercooled liquid condensate detrained from the shallow convection reduces the DJF (annual) Southern Ocean 30°–70°S ASR bias by 11.1 (6.5) W m^{-2} from 16.4 (7.3) to 5.3 W m^{-2} (0.8 W m^{-2}). The largest ASR bias reductions occur from 50° to 70°S, where detrained ice in the control (Figs. 1g–i) became detrained supercooled liquid in the experiment. In summary, the atmosphere-only model runs demonstrate that increasing the supercooled liquid in shallow convective clouds reduces midlatitude ocean ASR biases, especially over the Southern Ocean.

b. *Shortwave radiation bias reduction in fully coupled model runs*

Having demonstrated that we can substantially reduce midlatitude ocean ASR biases by decreasing T_{ice} in

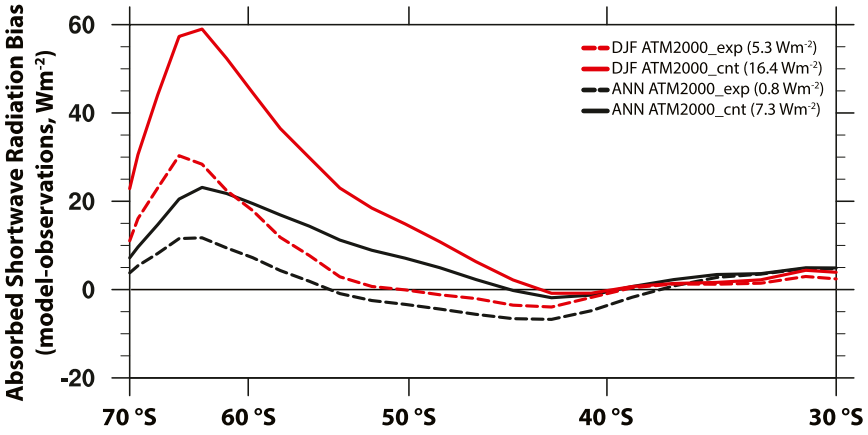

FIG. 4. Zonal mean absorbed shortwave radiation bias over the Southern Ocean in atmosphere-only runs. Values in parentheses indicate the total Southern Ocean (30°–70°S) bias. Observations are from CERES-EBAF (Loeb et al. 2009) version 2.8 (v2.8) for the years 2000–13. See Table 1 for model run descriptions. Both ANN and Southern Hemisphere summer (DJF) means are plotted.

atmosphere-only runs, we next evaluate the impacts of the same T_{ice} changes in fully coupled model runs. We begin by comparing global mean energy imbalance in a fully coupled experiment (FC1850_exp, T_{ice} = 253 K) with a fully coupled control (FC1850_cnt, T_{ice} = 268 K). While the control has a small positive TOA energy imbalance of 0.3 W m^{-2}, the experiment has a larger negative TOA energy imbalance of −0.9 W m^{-2}. This imbalance must be reduced to produce a stable coupled simulation. The negative global energy imbalance in the experiment results from strong shortwave cloud cooling (Table 2). Not surprisingly, the negative TOA energy imbalance in the experiment leads to sustained global cooling. After 29 years, the global mean temperature in the experiment decreases by 0.5 K and shows no sign of stopping. Worryingly, a similar experiment completed within a slab ocean framework experienced runaway global cooling of 40 K after 40 years with sea ice reaching the equator (not shown). Global cooling in this "snowball earth" run was enhanced by low-latitude shortwave cloud and sea ice feedbacks that were especially prominent after year 25 (not shown).

Decreasing T_{ice} has a large effect on ASR, which brings the model out of global energy balance. To obtain a stable fully coupled model run with the ASR bias reductions resulting from decreasing T_{ice}, additional model parameter changes are required. We found appropriate additional model parameter changes by performing an assessment of the regional contributions to global mean energy balance in CESM1(CAM5). Despite having large Southern Ocean ASR biases, the fully coupled control has a stable climate with a small

TABLE 2. Global annual averages for fully coupled model runs. Observations are from CERES-EBAF v2.8 (Loeb et al. 2009) and the University of Wisconsin climatology (UWisc; O'Dell et al. 2008). Root-mean-square differences between model runs and observations are provided in parentheses. See Table 1 for a description of model runs.

	Top-of-model energy imbalance (W m^{-2})	Shortwave cloud radiative effect (W m^{-2})	Longwave cloud radiative effect (W m^{-2})	Total cloud fraction (%)	Gridbox cloud liquid water path (g m^{-2})	Surface temperature (K)
CERES-EBAF 2000–13	—	−47.2	26.0	—	—	—
UWisc 1987–2000	—	—	—	—	87.2	—
FC1850_cnt years 1–29	0.3	−47.7 (13.4)	22.6 (6.2)	63.1	40.1 (60.9)	287.2
FC1850_exp years 1–29	−0.9	−49.9 (13.0)	23.0 (5.8)	64.4	45.4 (54.8)	286.6
FC1850_texp years 1–29	0.0	−46.6 (10.9)	22.3 (6.1)	62.9	44.0 (55.8)	287.5
FC1850_texp years 150–200	0.0	−46.7 (10.9)	22.3 (6.1)	62.9	44.0 (55.7)	287.5

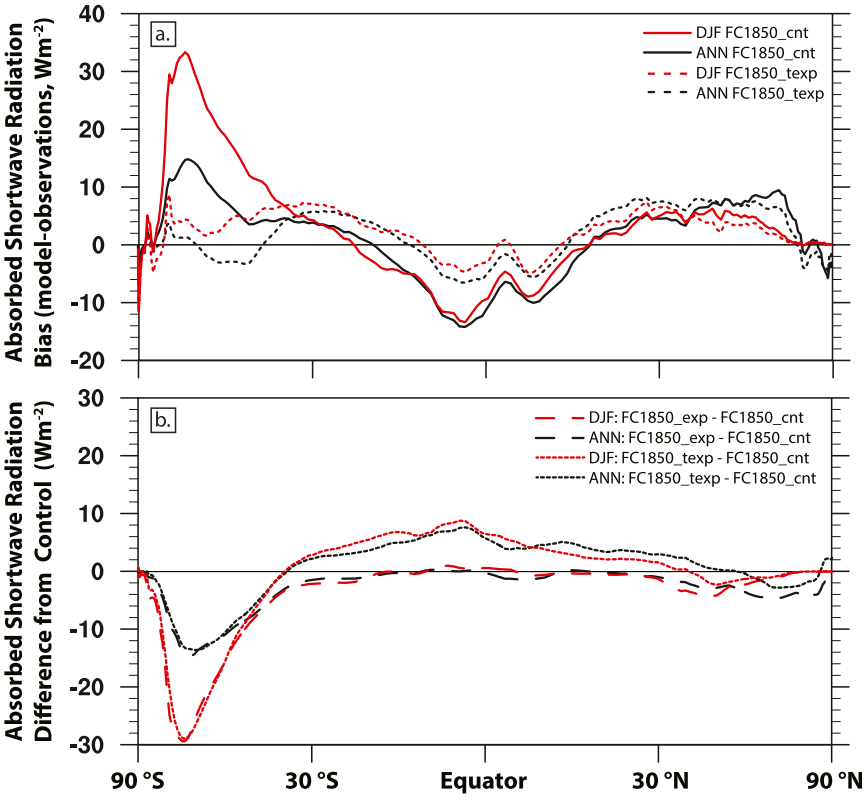

FIG. 5. Zonal global mean absorbed shortwave radiation in fully coupled runs: (a) bias and (b) difference from control (FC1850_cnt). Observations are from CERES-EBAF v2.8 (Loeb et al. 2009) for the years 2000–13. An area-weighted axis is used to show the balancing of midlatitude and tropical ASR biases and differences. See Table 1 for model run description. Both ANN and Southern Hemisphere summer (DJF) means are plotted.

global energy imbalance. The juxtaposition of a large Southern Ocean ASR bias and small global energy imbalance implies that the default version of CESM1(CAM5) achieves a globally balanced radiation budget with large compensating biases. Indeed, zonal mean plots of ASR bias for the control (Fig. 5a; FC1850_cnt, solid lines) show insufficient tropical ASR compensates for excessive midlatitude ASR in CESM1(CAM5), a common occurrence in climate models (Trenberth and Fasullo 2010). An exciting opportunity for both extratropical and tropical bias reduction emerges from globally compensating Southern Ocean and tropical ASR errors. If we can combine model parameter changes to increase tropical ASR with T_{ice} decreases to decrease Southern Ocean ASR, we can obtain a stable climate simulation with improved ASR in both the tropics and the midlatitudes.

To increase tropical ASR, we made two modifications to the threshold relative humidity for low cloud formation (rhminl; see supplemental information). First, we increased rhminl from the default value 0.8925–0.9175. Second, unlike in the control where rhminl over the land was 0.1 lower than rhminl over the ocean, we specified that the land have the same rhminl as the ocean. Both rhminl changes should be considered ''tuning'' (Mauritsen et al. 2012) to obtain global energy balance, as they were motivated by energy balance considerations and the desire for a stable coupled climate.

Having described the motivation to increase detrained supercooled liquid (decrease T_{ice}) and to tune the model (rhminl changes), we combine the T_{ice} and rhminl changes to obtain a fully coupled ''tuned experiment'' (FC1850_texp; Table 1). The fully coupled tuned experiment has a near-zero global energy imbalance and a stable global mean surface temperature that is similar to the fully coupled control (Table 2). Notably, the T_{ice} and rhminl changes in the tuned experiment produce a stable coupled climate with reduced ASR bias over both the Southern Ocean and the tropics (Fig. 5a and Table 2). Because the rhminl changes primarily affect low clouds, their impact on shortwave cloud cooling was larger than on longwave cloud warming (Table 2). The rhminl

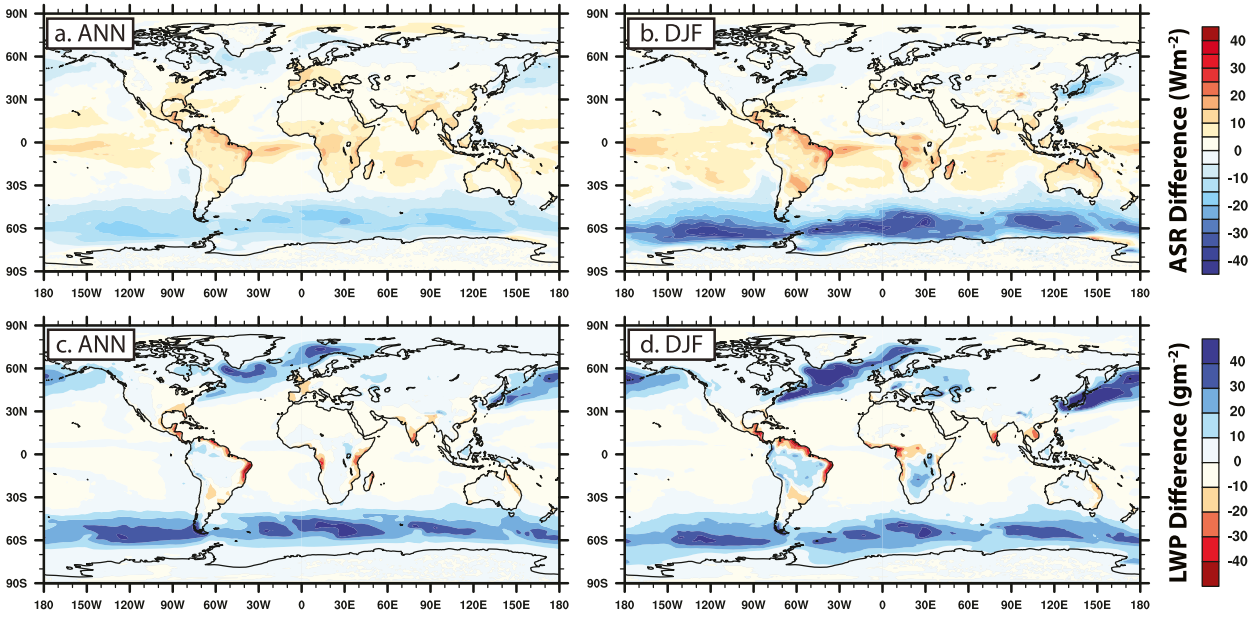

FIG. 6. Global difference maps for fully coupled climate model runs (FC1850_texp minus FC1850_cnt): (a) ANN ASR difference. (b) As in (a), but for DJF. (c) ANN gridbox mean cloud LWP difference. (d) As in (c), but for DJF. See Table 1 for model run description. An average of years 150–200 is shown for FC1850_texp, while an average of years 1–29 is shown for FC1850_cnt.

changes increased tropical ASR by reducing shortwave cloud cooling in the tuned experiment when compared to the control but had only a small impact on the extratropics (Fig. 5b). Confirming the zonal mean picture, global maps reveal that the largest LWP increases and ASR decreases in the fully coupled tuned experiment are over the Southern Ocean (Fig. 6). The fully coupled tuned experiment ASR reductions and LWP increases (Fig. 6) are similar to the atmosphere-only experiment (Fig. 3). In other words, we retained the desirable Southern Ocean ASR bias reduction in a fully coupled framework.

The climate of the fully coupled tuned experiment (FC1850_texp) quickly adjusts to the large radiation changes and reaches a new equilibrium climate state. Over the first 30 yr, the global ocean heat imbalance (a measure of ocean thermal disequilibrium) in FC1850_texp was small (0.06 W m^{-2}). During years 150–200 of FC1850_texp, the global ocean heat imbalance is an order of magnitude smaller (0.007 W m^{-2}) than during the first 30 yr of FC1850_texp. In addition, the global top-of-atmosphere imbalance remains small (<0.1 W m^{-2}) over the entire 200 yr of simulation of FC1850_texp. We did not find a large climate-relevant transient response over 200 yr of simulation. These results suggest that the 200-yr-long FC1850_texp simulation can be used to understand the fully coupled climate system response to brightening the Southern Ocean and dimming the tropics.

c. *Climate influence of shortwave radiation bias reduction in fully coupled model runs*

To evaluate the equilibrium climate system response to the ASR bias reductions shown in Fig. 5a, we next compare years 150–200 of the fully coupled tuned experiment (FC1850_texp) with the fully coupled control (FC1850_cnt). Figure 7 compares zonal mean air temperatures and zonal winds. Because of an enhanced meridional temperature gradient, the Southern Hemisphere jet strengthens in the tuned experiment as compared to the control. A stronger Southern Hemisphere jet is seen in all seasons, but especially in DJF (Fig. 7d). Small poleward jet shifts are also evident in the Southern Hemisphere. The maximum wind speed at 850 mb, often used to identify the eddy-induced jet, shifts poleward by 0.1° (from 51.9° to 52.1°S) in the annual mean and shifts poleward by 0.6° (from 50.9° to 51.5°S) in DJF.

The results shown thus far demonstrate that ASR bias reduction can alter global energy budgets, temperature gradients, and atmospheric circulation. These findings motivate an assessment of the influence of ASR bias reduction on global heat transport. Figure 8 shows northward heat transport in the control and tuned experiment, including a partitioning into the atmosphere and the ocean appropriate for equilibrium conditions [see appendix of Kay et al. (2012b) for methods]. Consistent with enhanced meridional temperature gradients, poleward heat transport increases in the tuned

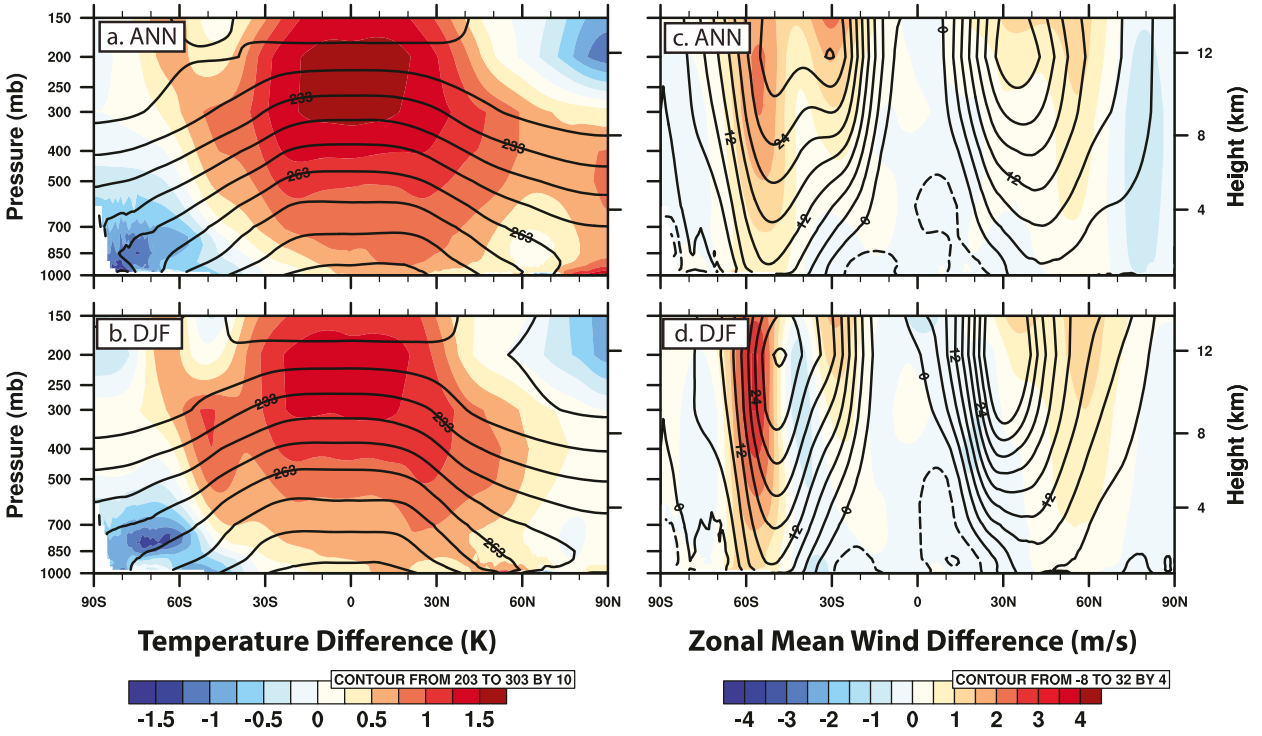

FIG. 7. Global zonal vertical mean temperature and circulation in fully coupled runs: (a) annual mean air temperature (black contours; FC1850_cnt) and temperature response (colors; FC1850_texp minus FC1850_cnt). (b) As in (a), but for DJF. (c) Annual zonal mean wind (black contours; FC1850_cnt) and zonal mean wind response (colors; FC1850_texp minus FC1850_cnt). (d) As in (c), but for DJF. See Table 1 for model run descriptions. An average of years 150–200 is shown for FC1850_texp, while an average of years 1–29 is shown for FC1850_cnt.

experiment as compared to the control. The Southern Hemisphere poleward heat transport increase is more than double the Northern Hemisphere poleward heat transport increase. In addition to interhemispheric magnitude differences, there are interhemispheric differences in the atmospheric and oceanic contributions to total heat transport change. In the Northern Hemisphere, poleward heat transport increases are due entirely to the atmosphere while, in the Southern Hemisphere, both the ocean (dominant in the tropics) and atmosphere (dominant in the midlatitudes) contribute to increased poleward heat transport.

We next examine the mechanisms underlying the increased poleward oceanic heat transport in the Southern Hemisphere in FC1850_texp as compared to FC1850_cnt. The increased Southern Hemisphere poleward ocean heat transport response emerges in the first 30 yr of FC1850_texp. This quick response implicates the shallow wind-driven ocean circulation, not the deep thermohaline ocean circulation. Figure 9 shows the control surface zonal wind stress climatology and wind stress response (FC1850_texp minus FC1850_cnt). Over the Southern Hemisphere subtropics, easterly wind stress increases, especially in the Pacific basin. Figure 10 shows the meridional overturning circulation climatology and response to the wind stress changes shown in Fig. 9. In the top 1000 m of the Southern Hemisphere subtropical ocean, there is a deepening and intensification of the shallow overturning ocean circulation. The enhanced easterly winds shown in Figs. 9b and 9c increase poleward Ekman transport, leading to increased poleward oceanic heat transport. There is also a poleward shift in the location of upwelling in the Southern Ocean. By comparing Figs. 9b and 10b based on years 1–30 of FC1850_texp and Figs. 9c and 10c based on years 150–200 of FC1850_texp, it is clear that this shallow wind-driven ocean circulation response emerged almost entirely in the first 30 yr and remains stable over 200 yr of coupled simulation. After 200 yr of simulation, changes in the deep ocean thermohaline circulation are small, second order, and have a minor impact on the ocean heat transport response in Fig. 8 (not shown).

Table 3 compares cross-equatorial heat transport and tropical precipitation in the fully coupled simulations. While both the atmosphere and the ocean contribute,

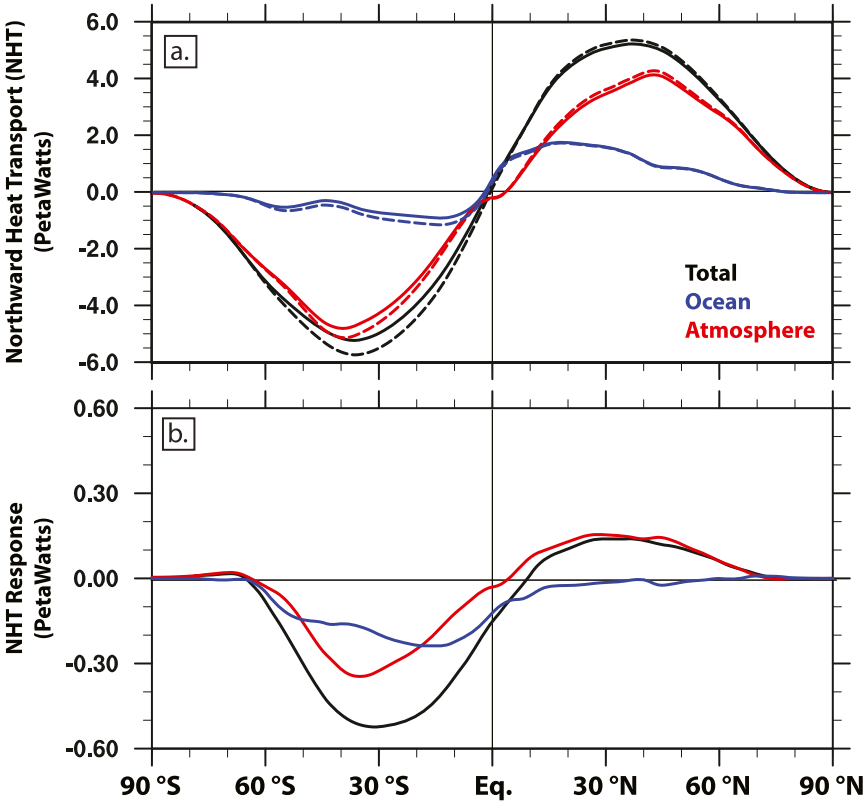

FIG. 8. Annual mean northward heat transport in fully coupled runs: (a) climatology in fully coupled control run (FC1850_cnt; solid) and tuned experiment (FC1850_texp; dashed); (b) response to increased detrainment of supercooled liquid in shallow convective clouds and tuning (FC1850_texp minus FC1850_cnt). See Table 1 for model run descriptions. An average of years 150–200 is shown for FC1850_texp, while an average of years 1–29 is shown for FC1850_cnt. Heat transport calculated using methods described in the appendix of Kay et al. (2012b). Total heat transport was calculated based on the fact that, in steady state, horizontal heat flux convergence across a latitude band is balanced by the net TOA flux poleward of that latitude. Ocean heat transport was calculated inline. Atmospheric heat transport was calculated by integrating the residual between the top-of-atmosphere and surface heat fluxes.

the ocean is responsible for 80% of the reductions in northward cross-equatorial heat transport in FC1850_texp as compared to FC1850_cnt. Consistent with a small change in atmospheric cross-equatorial heat transport, the tropical atmospheric circulation and precipitation responses are modest. Nevertheless, the sense of the responses is consistent with Hwang and Frierson (2013): ameliorating the Southern Ocean ASR bias reduces northward cross-equatorial atmospheric heat transport and shifts tropical precipitation northward, reducing the tropical precipitation asymmetry index bias. Unlike FC1850_cnt, atmospheric cross-equatorial heat transport in FC1850_texp is within the uncertainty bounds of modern observationally based estimates (Loeb et al. 2015). Yet the total and oceanic cross-equatorial heat transports are underestimated in FC1850_texp when compared with modern observationally based estimates. If comparison with modern observationally based estimates is appropriate, FC1850_texp has less realistic total and oceanic cross-equatorial heat transport than FC1850_cnt.

d. Influence of ocean heat transport on climate response to shortwave radiation bias reduction in slab ocean model runs

The results shown in Figs. 8–10 suggest that including dynamic ocean heat transport limits a proposed atmospheric teleconnection linking Southern Ocean ASR bias reduction with tropical precipitation shifts. Because slab ocean models are run with prescribed ocean heat transport, they provide a useful framework to quantify the influence of ocean heat transport on a modeled climate response. Leveraging the capability to prescribe ocean heat transport within SOMs, we next identify

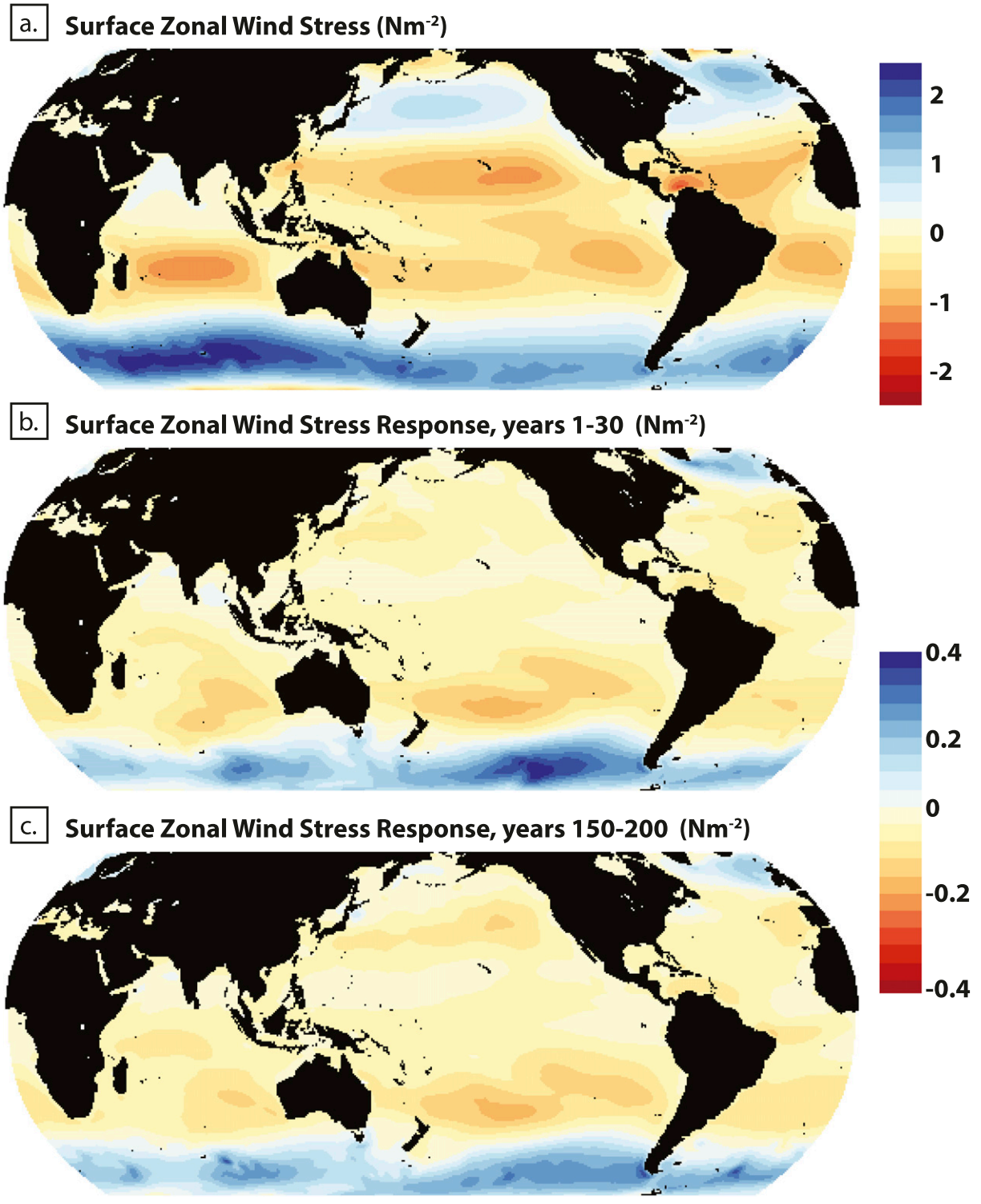

FIG. 9. Surface zonal wind stress and wind stress response: (a) climatology in fully coupled control (FC1850_cnt; years 1–29); (b) response to increased detrainment of supercooled liquid in shallow convective clouds and tuning (FC1850_texp minus FC1850_cnt) using years 1–30 of FC1850_texp. (c) As in (b), but using years 150–200 of FC1850_texp.

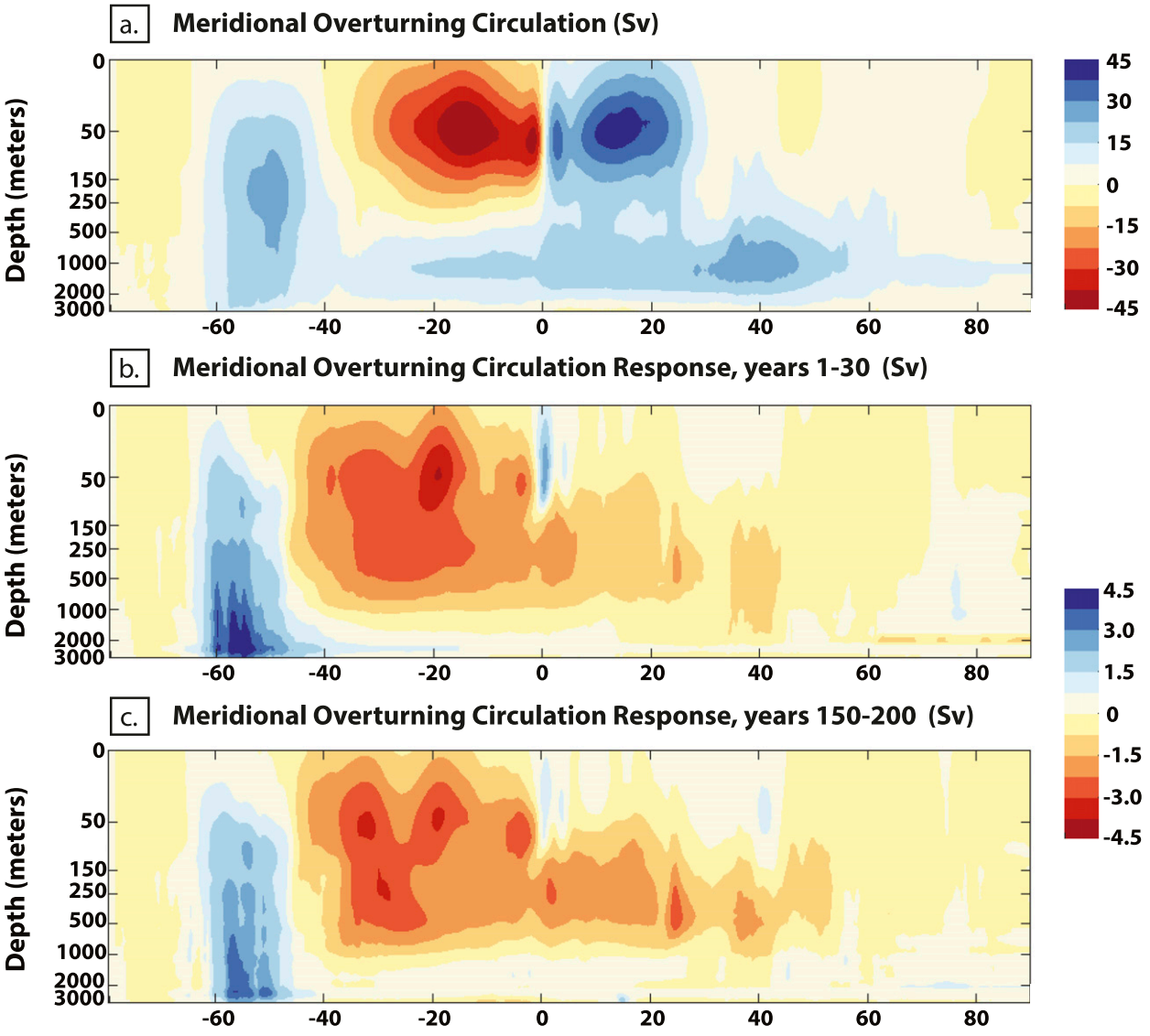

FIG. 10. Meridional overturning circulation (MOC; 1 Sv $\equiv 10^6\,m^3\,s^{-1}$): (a) climatology in fully coupled control (FC1850_cnt; years 1–29); (b) response to increased detrainment of supercooled liquid in shallow convective clouds and tuning (FC1850_texp minus FC1850_cnt) using years 1–30 of FC1850_texp. (c) As in (b), but using years 150–200 of FC1850_texp.

the influence of ocean heat transport on the climate response to ASR bias reduction. Specifically, we compare an SOM experiment with prescribed ocean heat transport changes resulting from ASR bias reduction (SOM1850_texp_ocnht=texp) to an SOM experiment with fixed ocean heat transport (SOM1850_texp_ocnht=cnt). Both SOM experiments have ASR bias reduction similar to the fully coupled experiment (Fig. 5).

We begin by comparing atmospheric heat transport in the SOMs and fully coupled runs (Fig. 11). Like the fully coupled experiment with dynamic ocean heat transport, the SOM experiment with changed ocean heat transport has small changes in cross-equatorial atmospheric heat transport. In contrast, the SOM with fixed ocean heat transport has large increases (0.3 PW) in atmospheric cross-equatorial heat transport. When ocean heat transport is fixed, ASR bias reduction produces increases in both northward cross-equatorial moisture transport and southward cross-equatorial energy transport (Fig. 11b).

If cross-equatorial atmospheric heat and moisture transport change (Fig. 11b), we expect a large tropical atmospheric circulation, moisture convergence, and precipitation response. Indeed, Figs. 12 and 13 confirm the importance of cross-equatorial atmospheric heat transport for shifting the ITCZ. When ocean heat transport is fixed, large cross-equatorial atmospheric

TABLE 3. Cross-equatorial heat transport (CHT) and tropical precipitation asymmetry index. The tropical precipitation asymmetry index (TPAI) is defined following Hwang and Frierson (2013) as precipitation in the Northern Hemisphere tropics (0°–20°N area averaged) minus precipitation in the Southern Hemisphere tropics (0°–20°S area averaged) normalized by the tropical mean precipitation (20°S–20°N area averaged). See Table 1 for a description of model runs.

	Total CHT (PW)	Atmospheric CHT (PW)	Oceanic CHT (PW)	Tropical precipitation asymmetry index
Observationally constrained 2001–12 (Loeb et al. 2015)	0.20 ± 0.05	−0.24 ± 0.04	0.44 ± 0.07	0.20
FC1850_cnt years 1–29	0.26	−0.18	0.44	0.11
FC1850_texp years 1–29	0.13	−0.19	0.32	0.12
FC1850_texp years 150–200	0.11	−0.21	0.32	0.15

heat transport changes occur. As a result, the tropical atmospheric response to reduced ASR includes reduced subsidence and increased precipitation north of the equator and enhanced subsidence and decreased precipitation south of the equator (Figs. 12a and 13). The tropical precipitation asymmetry index in SOM1850_tex_ocnht=cnt is 0.33, which is much larger than in FC1850_texp (0.15) or in modern-day observations (0.20) (Table 3). On the other hand, when ocean heat transport changes are predicted or prescribed, a muted tropical atmospheric circulation and precipitation response occurs (Figs. 12b,c and 13). These results confirm that, with dynamic ocean heat transport, tropical precipitation is less affected by Southern Ocean cooling. In

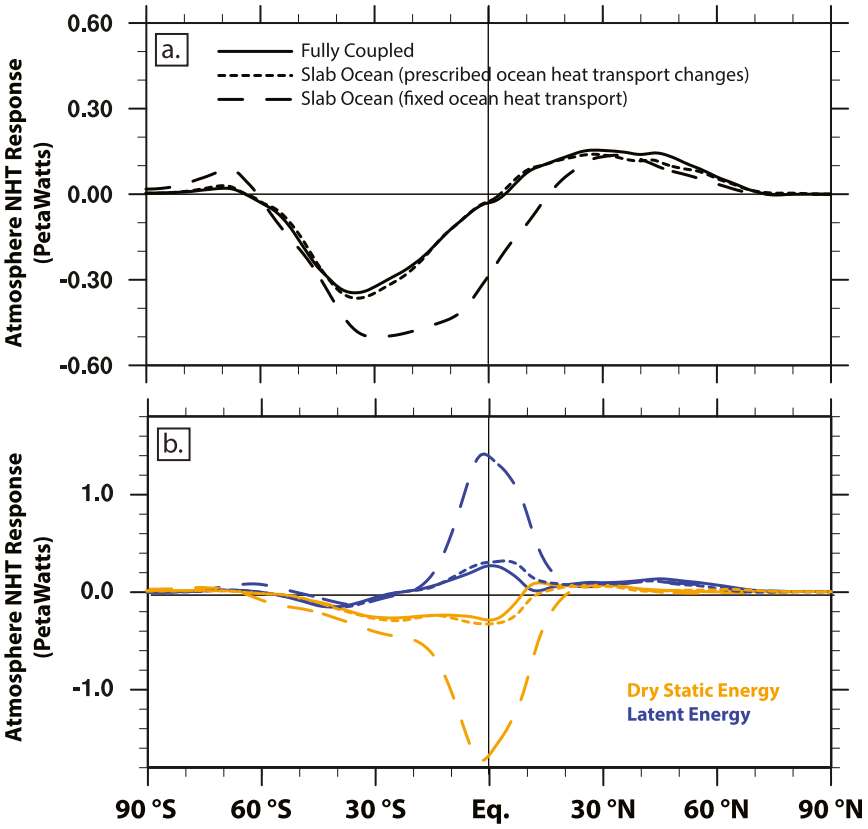

FIG. 11. Atmospheric northward heat transport response to increased detrainment of supercooled liquid in shallow convective clouds and tuning: (a) total energy and (b) latent and dry static energy. Responses are shown for fully coupled model (FC1850_texp minus FC1850_cnt), slab ocean model with prescribed ocean heat transport changes (SOM1850_texp_ocnht=texp minus SOM1850_cnt), and slab ocean model run with fixed ocean heat transport (SOM1850_texp_ocnht=cnt minus SOM1850_cnt). Years 1–20 are shown for all slab ocean experiments, years 1–29 are shown for FC1850_cnt, and years 150–200 are used for FC1850_texp. See Table 1 for model run descriptions.

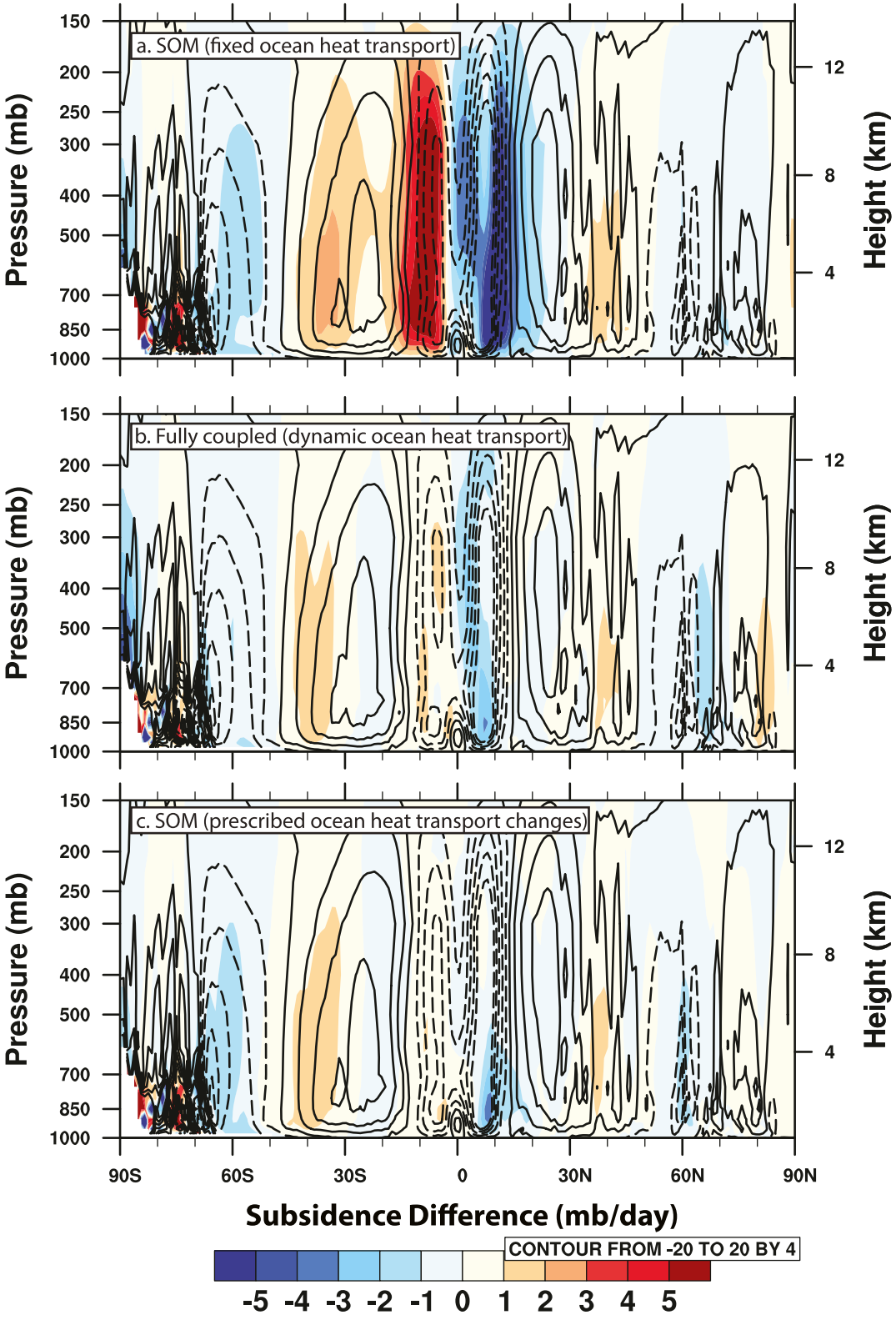

FIG. 12. Annual mean subsidence climatology (black contours) and subsidence response (colors): (a) slab ocean model run with fixed ocean heat transport (SOM1850_cnt and SOM1850_cnt minus SOM1850_texp_ocnht=cnt); (b) fully coupled model (FC1850_cnt and FC1850_texp minus FC1850_cnt); and (c) slab ocean model with prescribed ocean heat transport changes (SOM1850_cnt and SOM1850_cnt minus SOM1850_texp_ocnht=texp). Years 1–20 are shown for all slab ocean experiments, years 1–29 are shown for FC1850_cnt, and years 150–200 are used for FC1850_texp. See Table 1 for model run descriptions.

the climate model experiments with dynamic or prescribed ocean circulation changes, Southern Ocean ASR bias reduction leads to small ITCZ northward shifts because the ocean, not the atmosphere, dominates the cross-equatorial heat transport response. To summarize these results, Fig. 14 contains a schematic contrasting the climate impacts of ASR bias reduction with and without dynamic ocean heat transport.

4. Discussion

Our results demonstrate that shallow convective cloud phase exerts a strong control on global energy balance. Specifically, increasing supercooled liquid in shallow convective clouds to better match observations enables large reductions in long-standing shortwave radiation biases in a state-of-the-art climate model [CESM1(CAM5)]. The climate impacts of these shortwave radiation bias reductions are profound. A cooler, brighter Southern Ocean and warmer dimmer tropics leads to increased poleward heat transport, especially in the Southern Hemisphere. In response to stronger meridional temperature gradients, the Southern Hemisphere atmospheric jet increases in strength and shifts slightly poleward, as proposed by Ceppi et al. (2012). This jet strengthening and small poleward jet shift is consistent with a more poleward and realistic jet location in CESM1(CAM5) (Kay et al. 2014) when compared to other models of its class (Barnes and Polvani 2013). Unfortunately, the westerly winds over the Southern Ocean are already too strong in CESM1(CAM5), due in part to a cold upper-troposphere bias present in many models without a resolved stratospheric circulation (e.g., Charlton-Perez et al. 2013). Though fixing the Southern Ocean shortwave radiation bias is an important step forward and enables new science, it is not a panacea.

Yet, perhaps the most fundamental outcome of this study is a null result with relevance to climate dynamics. In our fully coupled tuned experiment, ITCZ shifts are small in response to a preferentially cooled Southern Hemisphere. Cooling the Southern Ocean has little impact on tropical precipitation because cross-equatorial heat transport changes occur primarily in the ocean (80% of the response), not the atmosphere (20% of the response). For this reason, quantifying the influence of Southern Ocean cooling on global climate requires the use of a model with dynamic ocean heat transport. Similarly, Deser et al. (2015) emphasize the importance of dynamic ocean heat transport and atmosphere–ocean coupling in producing the equatorially symmetric pattern of response to Arctic sea ice loss. More broadly, our results raise a critical question for the climate dynamics of extratropical–tropical teleconnections: Given interhemispheric temperature differences, when does the ocean, not the atmosphere, accomplish the required cross-equatorial heat transport? A dynamic ocean has been neglected in many (but not all) previous studies that analyzed atmospheric teleconnections and ITCZ shifts [e.g., Seo et al. 2014; Hwang and Frierson 2013, their supplementary materials; Frierson and Hwang 2012; some but not all references in Chiang and Friedman (2012)]. An important role for the ocean in cross-equatorial heat transport is certainly possible. For example, recent work has emphasized the importance of oceanic cross-equatorial heat transport in setting the mean position of the ITCZ (Frierson and Hwang 2012; Fučkar et al. 2013; Marshall et al. 2014). Slab ocean models are useful for isolating the role of dynamic ocean heat transport, but their use in quantifying global teleconnections should be justified via comparison with fully coupled model simulations.

While we have reduced a long-standing climate model bias, documented the climate response, and highlighted the role of dynamic ocean circulation in global teleconnections, important additional work remains. First of all, are our results robust in other models? Recent work using an independent fully coupled climate model (HadGEM2-ES) corroborates our finding that tropical rainfall is insensitive to Southern Hemispheric cooling (M. Hawcroft 2016, personal communication). Second, this study focuses on mean state 1850 climate, but more realistic shallow convective cloud phase in climate models also has implications for transient simulations and cloud–climate feedbacks. While the global mean cloud–climate feedback in response to increased greenhouse gases is likely positive (Boucher et al. 2013), negative Southern Ocean cloud feedbacks are present in most climate models (Zelinka et al. 2013), including CESM1(CAM5) (Kay et al. 2014). These negative cloud feedbacks are a consequence of optical depth increases (Zelinka et al. 2013), with a large contribution from clouds changing in phase from ice to liquid (Tsushima et al. 2006; Kay et al. 2014) and a small contribution from poleward jet shifts (Kay et al. 2014; Grise and Polvani 2014; Ceppi and Hartmann 2015). Yet, if cloud phase is diagnosed purely as a function of temperature in climate models [e.g., as it is within the shallow convection parameterization within CESM1(CAM5); see Eq. (1)], warming automatically converts ice to liquid and increases cloud optical depth. Two obvious follow-on questions emerge: First, could having more realistic liquid-dominated Southern Ocean clouds change the sign of the Southern Ocean cloud–climate feedback from negative to positive in CESM1(CAM5)? We expect the negative cloud feedback to be sensitive to both the amount of ice present in the mean state and its susceptibility to warming (McCoy et al. 2014). Second, how realistic are parameterizations that predict phase change purely as a function of temperature? The amount of

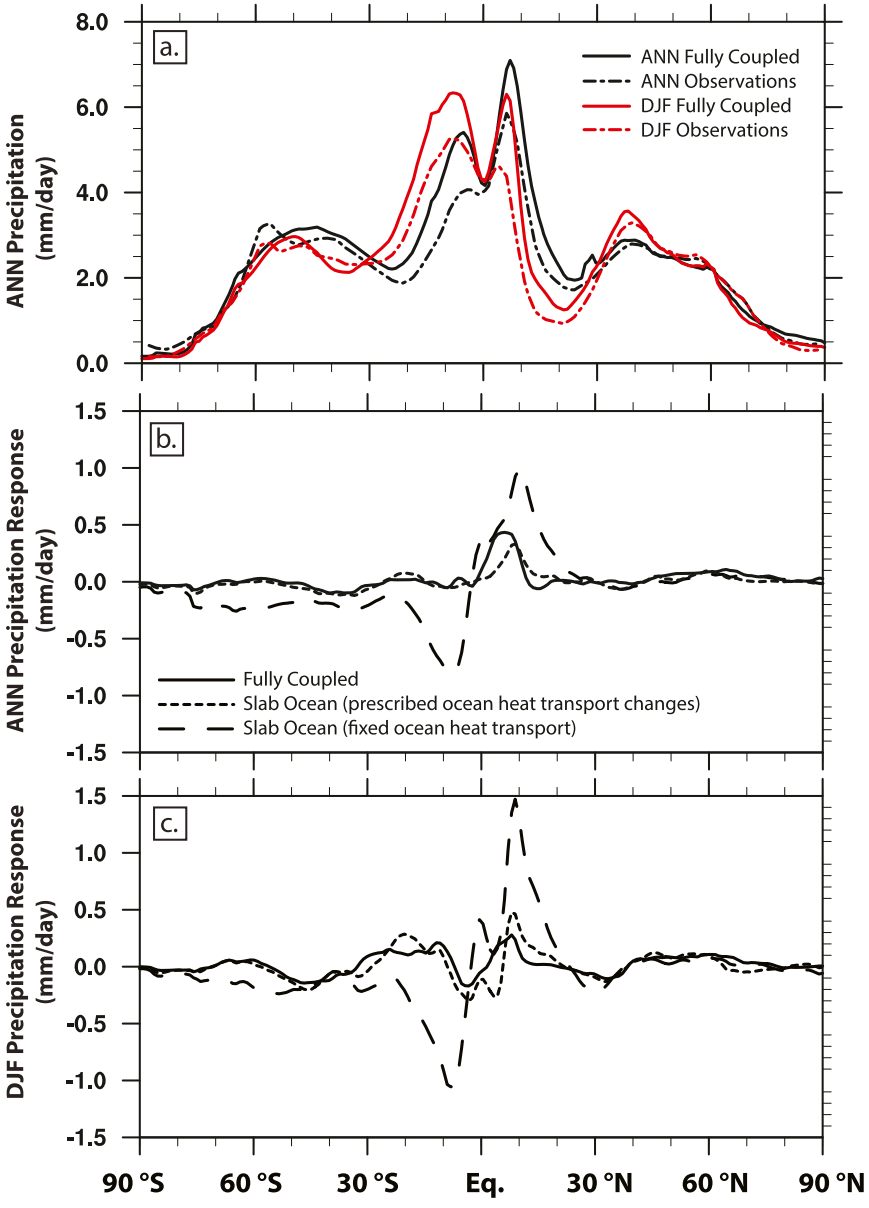

FIG. 13. Zonal annual mean precipitation (a) climatology in fully coupled control (FC1850_cnt; years 1–29) and Global Precipitation Climatology Project observations (1979–2009) (Adler et al. 2003); (b) ANN response; and (c) DJF response. Response is shown for fully coupled run (FC1850_texp minus FC1850_cnt), slab ocean model run with changes in ocean heat transport (SOM1850_texp_ocnht=texp minus SOM1850_cnt), and slab ocean model run without changes in ocean heat transport (SOM1850_texp_ocnht=cnt minus SOM1850_cnt). Years 1–20 are shown for all slab ocean experiments, years 1–29 are shown for FC1850_cnt, and years 150–200 are used for FC1850_texp. See Table 1 for model run descriptions.

liquid and ice in clouds in the real atmosphere depends on many factors beyond temperature (Morrison et al. 2012). Prognostic microphysical processes that predict cloud phase are increasingly common in models but are still often neglected in parameterized convection (e.g., Park et al. 2014; Forbes and Ahlgrimm 2014).

5. Summary

We reduced large, long-standing, and pervasive shortwave radiation model biases over the Southern Ocean and the tropics in a state-of-the-art global coupled climate model [CESM1(CAM5)]. Bias reductions

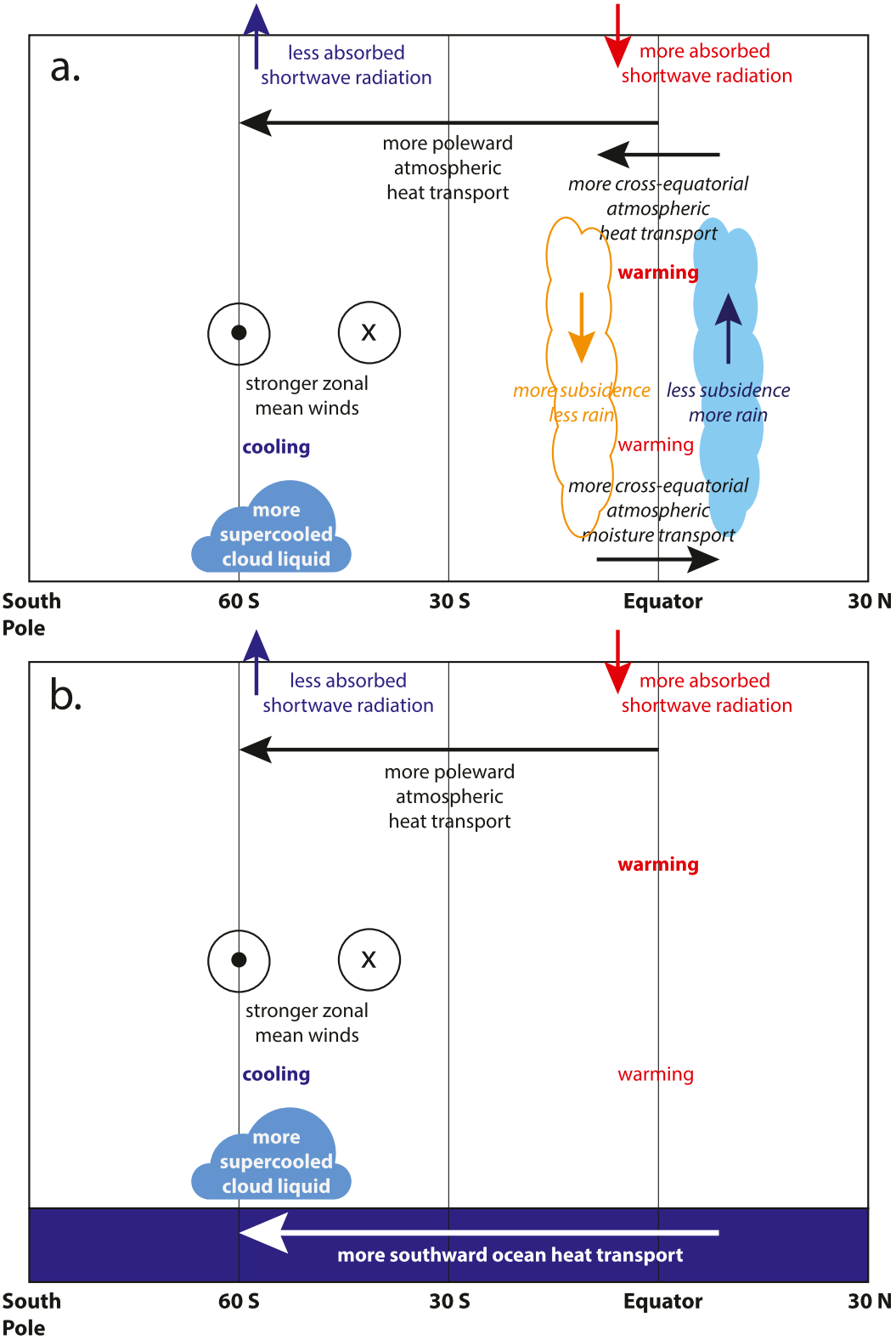

FIG. 14. Schematic showing climate response to absorbed shortwave radiation bias reduction (less ASR in Southern Ocean, more ASR in the tropics) (a) with fixed ocean heat transport and (b) with dynamic ocean heat transport. All indicated changes are anomalies relative to a mean state climate.

resulted from increasing the supercooled liquid water in shallow convective clouds to better match observations and tuning the relative humidity threshold for low clouds to obtain global energy balance. The climate impacts of the reduced shortwave radiation biases included a cooled Southern Ocean, a warmed tropics, increased poleward heat transport (especially in the Southern Hemisphere), and a stronger Southern Hemisphere atmospheric jet. Cooling the Southern Ocean had a negligible influence on tropical circulation and rainfall in our fully coupled model experiments. We found a weak extratropical–tropical atmospheric teleconnection in our fully coupled runs because Southern Ocean cooling increased cross-equatorial heat transport primarily in the ocean, not the atmosphere. More broadly, this work demonstrates the importance of using a global fully coupled model with dynamic ocean heat transport when quantifying the global climate impacts of interhemispheric temperature gradients. Future work will investigate the influence of more realistic cloud phase on transient climate simulations, including especially Southern Ocean shortwave cloud–climate feedbacks. Many important climate questions remain for the Southern Ocean.

Acknowledgments. The authors wish to thank Clara Deser, Andrew Gettelman, Matthew Woelfie, and Chris Bretherton for fruitful conversations related to this work, the Yellowstone CESM CSL for computing resources, and the scientists and software engineers that build CESM. This work was funded by start-up funds awarded to J. E. Kay by the University of Colorado Cooperative Institute for Research in Environmental Sciences (CIRES). P. Caldwell was supported by the Department of Energy's Office of Science Biological and Environmental Research Division Global Climate Modeling Group at Lawrence Livermore National Laboratory under Contract DE-AC52-07NA27344.

REFERENCES

Adler, R. F., and Coauthors, 2003: The Version-2 Global Precipitation Climatology Project (GPCP) Monthly Precipitation Analysis (1979–present). *J. Hydrometeor.*, **4**, 1147–1167, doi:10.1175/1525-7541(2003)004<1147:TVGPCP>2.0.CO;2.

Barnes, E. A., and L. M. Polvani, 2013: Response of the midlatitude jets and of their variability to increased greenhouse gases in the CMIP5 models. *J. Climate*, **26**, 7117–7135, doi:10.1175/JCLI-D-12-00536.1.

Bergeron, T., 1935: On the physics of clouds and precipitation. *Proces Verbaux de l'Association de Météorologie*, Paris, France, International Union of Geodesy and Geophysics, 156–178.

Bodas-Salcedo, A., K. D. Williams, P. R. Field, and A. P. Lock, 2012: The surface downwelling solar radiation surplus over the Southern Ocean in the Met Office model: The role of midlatitude cyclone clouds. *J. Climate*, **25**, 7467–7486, doi:10.1175/JCLI-D-11-00702.1.

——, and Coauthors, 2014: Origins of the solar radiation biases over the Southern Ocean in CFMIP2 models. *J. Climate*, **27**, 41–56, doi:10.1175/JCLI-D-13-00169.1.

——, P. G. Hill, K. Furtado, K. D. Williams, P. R. Field, J. C. Manners, P. Hyder, and S. Kato, 2016: Large contribution of supercooled liquid clouds to the solar radiation budget of the Southern Ocean. *J. Climate*, **29**, 4213–4228, doi:10.1175/JCLI-D-15-0564.1.

Boucher, O. D., and Coauthors, 2013: Clouds and aerosols. *Climate Change 2013: The Physical Science Basis*, T. F. Stocker et al., Eds., Cambridge University Press, 571–658. [Available online at http://www.climatechange2013.org/images/report/WG1AR5_Chapter07_FINAL.pdf.]

Ceppi, P., and D. L. Hartmann, 2015: Connections between clouds, radiation, and midlatitude dynamics: A review. *Curr. Climate Change Rep.*, **1**, 94–102, doi:10.1007/s40641-015-0010-x.

——, Y.-T. Hwang, D. M. W. Frierson, and D. L. Hartmann, 2012: Southern Hemisphere jet latitude biases in CMIP5 models linked to shortwave cloud forcing. *Geophys. Res. Lett.*, **39**, L19708, doi:10.1029/2012GL053115.

Cesana, G., and H. Chepfer, 2013: Evaluation of the cloud thermodynamic phase in a climate model using CALIPSO-GOCCP. *J. Geophys. Res. Atmos.*, **118**, 7922–7937, doi:10.1002/jgrd.50376.

Charlton-Perez, A. J., and Coauthors, 2013: On the lack of stratospheric dynamical variability in low-top versions of the CMIP5 models. *J. Geophys. Res. Atmos.*, **118**, 2494–2505, doi:10.1002/jgrd.50125.

Chiang, J. C. H., and A. R. Friedman, 2012: Extratropical cooling, interhemispheric thermal gradients, and tropical climate change. *Annu. Rev. Earth Planet. Sci.*, **40**, 383–412, doi:10.1146/annurev-earth-042711-105545.

Chubb, T. H., J. B. Jensen, S. T. Siems, and M. J. Manton, 2013: In situ observations of supercooled liquid clouds over the Southern Ocean during the HIAPER Pole-to-Pole Observation campaigns. *Geophys. Res. Lett.*, **40**, 5280–5285, doi:10.1002/grl.50986.

Deser, C., R. A. Tomas, and L. Sun, 2015: The role of ocean–atmosphere coupling in the zonal-mean atmospheric response to Arctic sea ice loss. *J. Climate*, **28**, 2168–2186, doi:10.1175/JCLI-D-14-00325.1.

Findeisen, W., 1938: Kolloid-meteorologische Vorgänge bei Neiderschlags-bildung. *Meteor. Z.*, **55**, 121–133.

Forbes, R. M., and M. Ahlgrimm, 2014: On the representation of high-latitude boundary layer mixed-phase cloud in the ECMWF global model. *Mon. Wea. Rev.*, **142**, 3425–3445, doi:10.1175/MWR-D-13-00325.1.

Frierson, D. M. W., and Y.-T. Hwang, 2012: Extratropical influence on ITCZ shifts in slab ocean simulations of global warming. *J. Climate*, **25**, 720–733, doi:10.1175/JCLI-D-11-00116.1.

Fučkar, N. S., S.-P. Xie, R. Farneti, E. A. Maroon, and D. M. W. Frierson, 2013: Influence of the extratropical ocean circulation on the intertropical convergence zone in an idealized coupled general circulation model. *J. Climate*, **26**, 4612–4629, doi:10.1175/JCLI-D-12-00294.1.

Gettelman, A., H. Morrison, S. Santos, P. Bogenschutz, and P. M. Caldwell, 2015: Advanced two-moment bulk microphysics for global models. Part II: Global model solutions and aerosol–cloud interactions. *J. Climate*, **28**, 1288–1307, doi:10.1175/JCLI-D-14-00103.1.

Grise, K. M., and L. M. Polvani, 2014: Southern Hemisphere cloud–dynamics biases in CMIP5 models and their implications for climate projections. *J. Climate*, **27**, 6074–6092, doi:10.1175/JCLI-D-14-00113.1.

Hu, Y., S. Rodier, K. Xu, W. Sun, J. Huang, B. Lin, P. Zhai, and D. Josset, 2010: Occurrence, liquid water content, and fraction of supercooled water clouds from combined CALIOP/IIR/MODIS measurements. *J. Geophys. Res.*, **115**, D00H34, doi:10.1029/2009JD012384.

Huang, Y., S. T. Siems, M. J. Manton, A. Protat, and J. Delanoë, 2012: A study on the low-altitude clouds over the Southern Ocean using the DARDAR-MASK. *J. Geophys. Res.*, **117**, D18204, doi:10.1029/2012JD017800.

Hurrell, J., and Coauthors, 2013: The Community Earth System Model: A framework for collaborative research. *Bull. Amer. Meteor. Soc.*, **94**, 1339–1360, doi:10.1175/BAMS-D-12-00121.1.

Hwang, Y.-T., and D. M. W. Frierson, 2013: A link between the double-Intertropical Convergence Zone problem and cloud biases over the Southern Ocean. *Proc. Natl. Acad. Sci. USA*, **110**, 4935–4940, doi:10.1073/pnas.1213302110.

Kay, J. E., and Coauthors, 2012a: Exposing global cloud biases in the Community Atmosphere Model (CAM) using satellite observations and their corresponding instrument simulators. *J. Climate*, **25**, 5190–5207, doi:10.1175/JCLI-D-11-00469.1.

——, M. M. Holland, C. Bitz, E. Blanchard-Wrigglesworth, A. Gettelman, A. Conley, and D. Bailey, 2012b: The influence of local feedbacks and northward heat transport on the equilibrium Arctic climate response to increased greenhouse gas forcing in coupled climate models. *J. Climate*, **25**, 5433–5450, doi:10.1175/JCLI-D-11-00622.1.

——, B. Medeiros, Y.-T. Hwang, A. Gettelman, J. Perket, and M. G. Flanner, 2014: Processes controlling Southern Ocean shortwave climate feedbacks in CESM. *Geophys. Res. Lett.*, **41**, 616–622, doi:10.1002/2013GL058315.

——, and Coauthors, 2015: The Community Earth System Model (CESM) Large Ensemble Project: A community resource for studying climate change in the presence of internal climate variability. *Bull. Amer. Meteor. Soc.*, **96**, 1333–1349, doi:10.1175/BAMS-D-13-00255.1.

——, L. Bourdages, N. B. Miller, A. Morrison, V. Yettella, H. Chepfer, and B. Eaton, 2016: Evaluating and improving cloud phase in the Community Atmosphere Model version 5 using spaceborne lidar observations. *J. Geophys. Res. Atmos.*, **121**, 4162–4176, doi:10.1002/2015JD024699.

Lin, J.-L., 2007: The double-ITCZ problem in IPCC AR4 coupled GCMs: Ocean–atmosphere feedback analysis. *J. Climate*, **20**, 4497–4525, doi:10.1175/JCLI4272.1.

Loeb, N. G., B. A. Wielicki, D. R. Doelling, G. L. Smith, D. F. Keyes, S. Kato, N. Manalo-Smith, and T. Wong, 2009: Toward optimal closure of the Earth's top-of-atmosphere radiation budget. *J. Climate*, **22**, 748–766, doi:10.1175/2008JCLI2637.1.

——, H. Wang, A. Cheng, S. Kato, J. T. Fasullo, K. Xu, and R. P. Allan, 2015: Observational constraints on atmospheric and oceanic cross-equatorial heat transports: Revisiting the precipitation asymmetry problem in climate models. *Climate Dyn.*, **46**, 3239–3257, doi:10.1007/s00382-015-2766-z.

Marshall, J., A. Donohoe, D. Ferreira, and D. McGee, 2014: The ocean's role in setting the mean position of the Inter-Tropical Convergence Zone. *Climate Dyn.*, **42**, 1967–1979, doi:10.1007/s00382-013-1767-z.

Mauritsen, T., and Coauthors, 2012: Tuning the climate of a global model. *J. Adv. Model. Earth Syst.*, **4**, M00A01, doi:10.1029/2012MS000154.

McCoy, D. T., D. L. Hartmann, and D. P. Grosvenor, 2014: Observed Southern Ocean cloud properties and shortwave reflection. Part II: Phase changes and low cloud feedback. *J. Climate*, **27**, 8858–8868, doi:10.1175/JCLI-D-14-00288.1.

Morrison, A. E., S. T. Siems, and M. J. Manton, 2011: A three-year climatology of cloud-top phase over the Southern Ocean and North Pacific. *J. Climate*, **24**, 2405–2418, doi:10.1175/2010JCLI3842.1.

Morrison, H., and A. Gettelman, 2008: A new two-moment bulk stratiform cloud microphysics scheme in the NCAR Community Atmosphere Model, version 3 (CAM3). Part I: Description and numerical tests. *J. Climate*, **21**, 3642–3659, doi:10.1175/2008JCLI2105.1.

——, G. de Boer, G. Feingold, J. Harrington, M. D. Shupe, and K. Sulia, 2012: Resilience of persistent Arctic mixed-phase clouds. *Nat. Geosci.*, **5**, 11–17, doi:10.1038/ngeo1332.

O'Dell, C. W., F. J. Wentz, and R. Bennartz, 2008: Cloud liquid water path from satellite-based passive microwave observations: A new climatology over the global oceans. *J. Climate*, **21**, 1721–1739, doi:10.1175/2007JCLI1958.1.

Park, S., and C. S. Bretherton, 2009: The University of Washington shallow convection and moist turbulence schemes and their impact on climate simulations with the Community Atmosphere Model. *J. Climate*, **22**, 3449–3469, doi:10.1175/2008JCLI2557.1.

——, ——, and P. J. Rasch, 2014: Integrating cloud processes in the Community Atmosphere Model, version 5. *J. Climate*, **27**, 6821–6856, doi:10.1175/JCLI-D-14-00087.1.

Schneider, T., T. Bischoff, and G. H. Haug, 2014: Migrations and dynamics of the intertropical convergence zone. *Nature*, **513**, 45–53, doi:10.1038/nature13636.

Seo, J., S. M. Kang, and D. M. W. Frierson, 2014: Sensitivity of intertropical convergence zone movement to the latitudinal position of thermal forcing. *J. Climate*, **27**, 3035–3042, doi:10.1175/JCLI-D-13-00691.1.

Shupe, M. D., and J. M. Intrieri, 2004: Cloud radiative forcing of the Arctic surface: The influence of cloud properties, surface albedo, and solar zenith angle. *J. Climate*, **17**, 616–628, doi:10.1175/1520-0442(2004)017<0616:CRFOTA>2.0.CO;2.

Taylor, K. E., R. J. Stouffer, and G. A. Meehl, 2012: An overview of CMIP5 and the experiment design. *Bull. Amer. Meteor. Soc.*, **93**, 485–498, doi:10.1175/BAMS-D-11-00094.1.

Trenberth, K. E., and J. T. Fasullo, 2010: Simulation of present-day and twenty-first-century energy budgets of the southern oceans. *J. Climate*, **23**, 440–454, doi:10.1175/2009JCLI3152.1.

Tsushima, Y., and Coauthors, 2006: Importance of the mixed-phase cloud distribution in the control climate for assessing the response of clouds to carbon dioxide increase: A multi-model study. *Climate Dyn.*, **27**, 113–126, doi:10.1007/s00382-006-0127-7.

Wegener, A., 1911: *Thermodynamik der Atmosphäre*. Leipzig, 331 pp.

Williams, K. D., and Coauthors, 2013: The Transpose-AMIP II experiment and its application to the understanding of Southern Ocean cloud biases in climate models. *J. Climate*, **26**, 3258–3274, doi:10.1175/JCLI-D-12-00429.1.

Zelinka, M. D., S. A. Klein, K. E. Taylor, T. Andrews, M. J. Webb, J. M. Gregory, and P. M. Forster, 2013: Contributions of different cloud types to feedbacks and rapid adjustments in CMIP5. *J. Climate*, **26**, 5007–5027, doi:10.1175/JCLI-D-12-00555.1.